Available online at www.sciencedirect.com
SCIENCE DIRECT®
Nuclear Instruments and Methods in Physics Research A 547 (2005) 302–312
NUCLEAR INSTRUMENTS & METHODS IN PHYSICS RESEARCH Section A
www.elsevier.com/locate/nima

The development and beam test of an RF chopper system for J-PARC

Sheng Wang[a,*], Shinian Fu[a], Takao Kato[b]

[a]*Institute of High Energy Physics, P.O. Box 918, Beijing 100049, People's Republic of China*
[b]*KEK, High Energy Accelerator Research Organization, Accelerator Division, 1-1 Oho, Tsukuba-shi, Ibaraki-ken 305-0801, Japan*

Received 22 April 2004; received in revised form 23 February 2005; accepted 30 March 2005
Available online 25 May 2005

Abstract

The linac of the Japan Proton Accelerator Research Complex (J-PARC) is now under construction. It is a high-intensity linac with a peak H^- current of 50 mA and a 1.25% duty factor. As a key component of the medium-energy beam-transport line of the linac, a chopper is necessary to obtain the required beam structure for the following 3-GeV rapid-cycling synchrotron, and also plays an important role in beam-loss control in such a high-intensity accelerator. Clean chopping requires a short rise time and a high deflecting field. An radio frequency deflector (RFD) was proposed as a chopper for the J-PARC linac, because of its merits of high deflecting field, compact structure, ease to manufacture and both reliability and flexibility of the total chopper operation. An RF chopper, consisting of two RFDs, has been developed. In a low-level RF test, the fundamental RF properties show good agreement with those of a simulation in the design. In a high-power test, the chopper works well without any discharge under 36 kW peak driving power. In a test of the coupled RFD system, the longer rise time of the second RFD and the delay of the second RFD excitation were observed. A beam test of the RF chopper was also successfully performed up to a peak current of 25 mA. The chopper system worked very stable during the beam test, and the sufficient separation between chopped and normal beam was obtained, with a short rise/fall time (10 ns) of the chopped beam.

PACS: 29.27.Eg

Keywords: J-PARC; RF chopper; Frequency tuning; Rise time; Proton linac; Beam test

1. Introduction

The Japan Proton Accelerator Research Complex (J-PARC) consists of a 400-MeV H^- linac, a 3-GeV rapid-cycling synchrotron (RCS) and a 50-GeV synchrotron (main ring) [1]. As an injector

*Corresponding author. Tel.: +86 10 88235201; fax: +86 10 88236190.
E-mail address: wangs@ihep.ac.cn (S. Wang).

0168-9002/$ - see front matter © 2005 Elsevier B.V. All rights reserved.
doi:10.1016/j.nima.2005.03.144

of J-PARC, the linac provides a 50 mA peak current with a duty factor of 1.25%. This includes a H^- ion source, a 3-MeV radio frequency quadrupole linac (RFQ), a 50-MeV drift tube linac (DTL), a 200-MeV separated-type drift tube linac (SDTL), a 400-MeV annular coupled structure linac (ACS), and a 3-MeV medium-energy beam transport line (MEBT) between RFQ and DTL. MEBT accomplishes beam matching and chopping. In the J-PARC project, 500 μs long macropulses from the ion source need to be chopped into sub-pulses for injecting into the following 3-GeV rapid-cycling ring. Fig. 1 shows the required time structure of the macro- and microbeam pulses. The chopped pulse should have a clean cut at the head and the tail of the pulse so as to avoid beam losses at later parts of the linac, or during injection into the ring. An RF deflector (RFD) was proposed [2] and designed [3] as a chopper for the J-PARC linac, because of its merits of having a high deflecting field, a compact structure, ease to manufacture and both reliability and flexibility of the total chopper operation. An RF chopper, consisting of two RFDs, has been successfully developed. In a low-level RF test, the fundamental RF properties show good agreement with those in a design simulation. In a high-power test, the chopper worked well without any discharge under 36 kW peak driving power, and the longer rise time of the second RFD and the delay of the second RFD excitation were observed in the coupled RFD system. A beam test of the RF chopper was also successfully performed up to a peak current of 25 mA, which is limited by the ion source during the experiment. Some results of the beam test are also described in this paper.

2. The improvement of the RFD cavity design

RFD is operated in a TE_{11}-like mode at 324 MHz. The cavity wall consists of two parts: the open cavity body and two cover plates. On each plate there is a large coupling loop. Inside the cavity, two electrodes are adopted to generate the deflecting electric field, and two beam pipes are designed to shield the beam from a reverse deflecting effect of the magnetic field. The geometry of the cavity is plotted in Fig. 2. We use two large coupling loops in order to reach a fast rise/

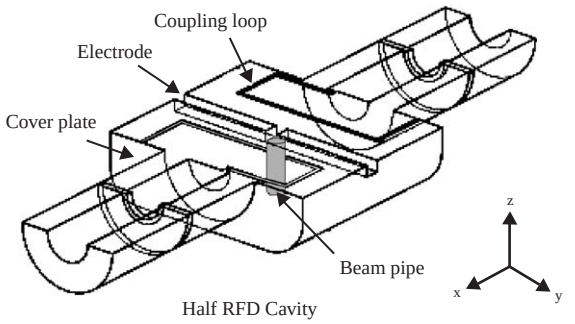

Fig. 2. Geometric sketch of an RFD cavity (beam goes in the z direction).

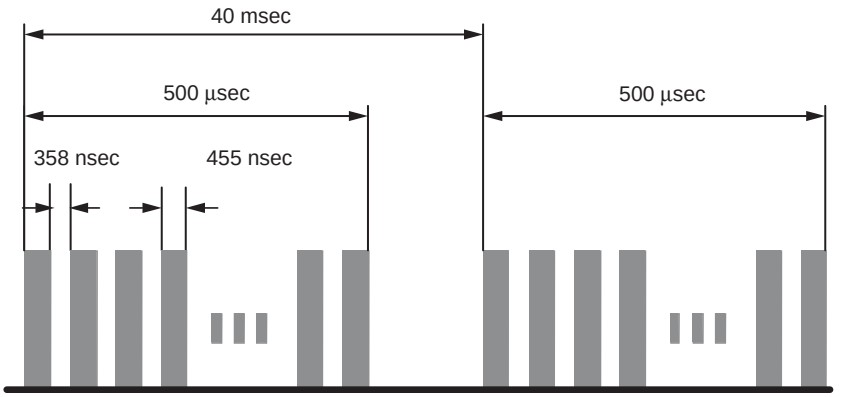

Fig. 1. Required time structure of the macro- and microbeam pulses.

fall time of the deflecting field in the RFD cavity. To save the MEBT space, two RFDs (RFD-A and RFD-B) were constructed as a whole to form a RF chopper, as shown in Fig. 3 [1].

It was found that the fabricated RFD cavity has a frequency shift of about 2 MHz from the design value, and it cannot be corrected by a tuner without negligible effects on the field distribution in the cavity. Although the bandwidth is very large (~30 MHz), the frequency deviation still induces some negative effects: additional reflection, deformation of the waveform and a mismatch between two RFDs in the coupled RFD system. For example, Fig. 4 shows the deformed waveform of the first RFD (RFD-A) when such a mismatch exists in the coupled RFD system. To tune the resonant frequency back to 324 MHz and to keep the bandwidth and other parameters unchanged, a new coupling loop has been designed based on the HFSS simulation. This tuning method has two merits: easy fabrication and less cost. By adopting a different size of the coupling loops for two RFDs, respectively, the resonant frequencies of two chopper cavities were tuned to 324 MHz. The RF measurement results show a good performance of the modified coupled RFD system [4]. Table 1 indicates the parameters of the RFD measured with the old loop and the new one, respectively. All of the test results of the RFD given in the following parts of this paper are based on the new coupling loop. Fig. 5 depicts the waveform from the first RFD of the coupled RFD system in the high-power test. It shows that there is no mismatch between two RFD cavities in the coupled RFD

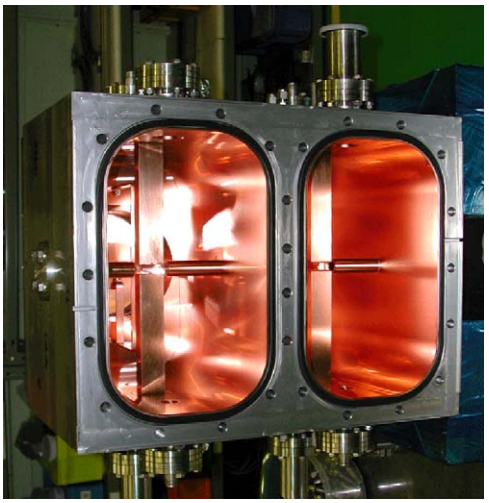

Fig. 3. Fabricated RF chopper formed by two RFDs with opening cover plates in one side.

Table 1
Measured parameters with old and new coupling loops

	Resonant frequency (MHz)		Bandwidth (MHz)
	RFD-A	RFD-B	
Old loop	322.30	321.90	30
New loop	324.00	324.15	30

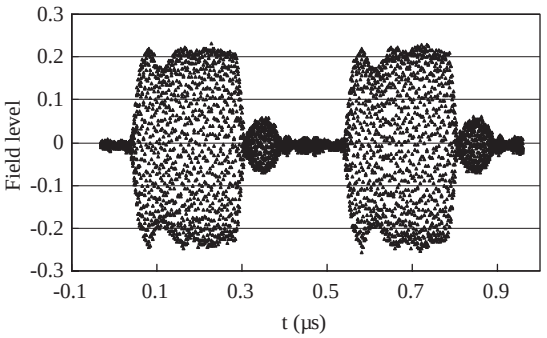

Fig. 4. Deformed waveform of the RFD-A of a coupled system due to mismatch (36 kW driving power).

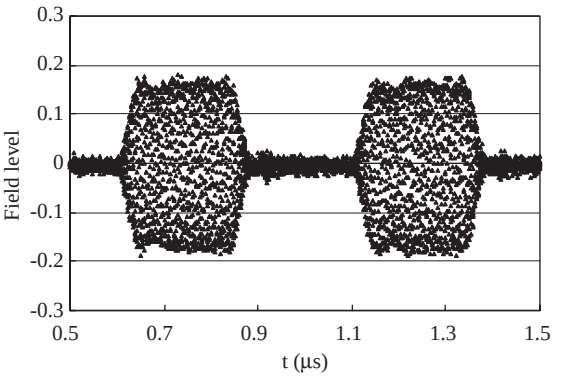

Fig. 5. Waveform in the RFD-A of a coupled RFD system without mismatch (36 kW driving power).

system, after the resonant frequency is tuned to the operating frequency.

For tuning the frequency, a tuner was installed in each RFD cavity. In the measurement and simulation, a default value of 15 mm insertion of the tuner was set. The allowable tuning range of the cavity is −250 to 550 kHz, corresponding to a tuner insertion from 0 to 25 mm.

3. The test of single RFD cavity

3.1. Measurement of the RFD cavity with small coupling loops

The fundamental RF properties were measured with small RF couplers, instead of using large coupling loops. Table 2 lists the measured frequencies and the unloaded Q values. Mode 1 corresponds to the deflecting one. Since the calculated Q value is about 11,000, the obtained results were satisfactory.

Table 2
Measured results with small RF couplers

	RFD-A		RFD-B	
	Frequency (MHz)	Q	Frequency (MHz)	Q
Mode 1	322.275	9760	321.849	9720
Mode 2	401.916	9520	402.118	9800
Mode 3	930.349	11500	930.526	13500
Mode 4	992.514	26700	992.255	27200

3.2. The measurement of the RFD cavity with large coupling loops

To reach a very fast rise/fall time, large coupling loops were used in the RFD. The scattering parameters were measured by a network analyzer. Fig. 6a gives the measured scattering parameter (S_{21}) versus the frequency of the single RFD with large coupling loops. It shows that the resonant frequency is 324 MHz, with a 30 MHz bandwidth at −3 dB; a loaded Q-value of 10.8 was achieved, corresponding to a cavity rise time of 11 ns. As a comparison, Fig. 6b gives the corresponding simulated results by HFSS. It indicates a resonant frequency of 324 MHz and a bandwidth of 30 MHz at −3 dB. The measured parameters agree very well with the simulated values.

3.3. High-power test of the single RFD cavity

Taking advantage of high reliability and high stability, the solid-state-type power amplifier was chosen as the power source of the chopper. A 30-kW solid-state power amplifier was successfully constructed [5]. It consists of 30 power modules, and each module produces an RF power of more than 1 kW, and the maximum output power reaches 36 kW. The output rise/fall time of the amplifier is about 15 ns. Because a large output coupling loop was adopted for obtaining a low loaded Q value, most of the power is coupled out of the cavity instead of being dissipated inside the cavity. A 50 Ω matching load is used as the absorbing load.

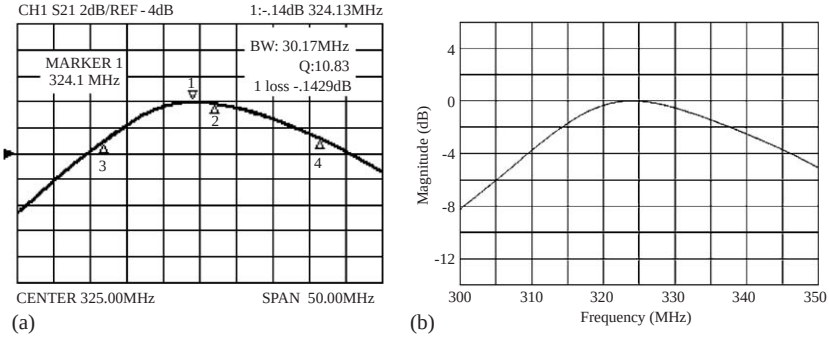

Fig. 6. (a) Measured scattering parameter S_{21}. The resonant frequency is 324.12 MHz and the bandwidth is 30 MHz. The loaded Q is 10.8. (b) Simulated scattering parameter by HFSS. The resonant frequency is 324 MHz with the same bandwidth of 30 MHz.

A high-power test of the RFD was successfully performed. The RFD worked very well without any discharge up to a 36 kW peak driving power. There are water cooling channels in the cover plates of the cavity and the two electrodes, but no cooling in the wall of the cavity. The variation in the temperature at the wall of the cavity was less than 0.3° under different input power and duty factors during high-power tests. The stability of the temperature benefits from the small percentage of dissipation of the power in the cavity and relatively small average driving power.

3.4. Measurement of rise/fall time of the single RFD cavity

According to the measured loaded Q value (Q_L), as shown in Fig. 6a, the rise time of the cavity is $Q_L/\pi f_0 = 10.6$ ns, in which f_0 is the resonant frequency. The rise time of the whole RFD system is longer than that of the cavity, because of the contribution from the amplifier. Fig. 7 depicts the measured RF response of the RFD cavity during the rise time of the RFD system. The measured rise time of the RFD system, the field level from 10% to 90%, is about 27 ns, or 9 RF periods, which includes a 15-ns contribution from the amplifier. To verify the contribution of the power amplifier to the rise time of the RFD system, a low-level RF-signal source with a much faster rise time of 2 RF periods was used in measurement and

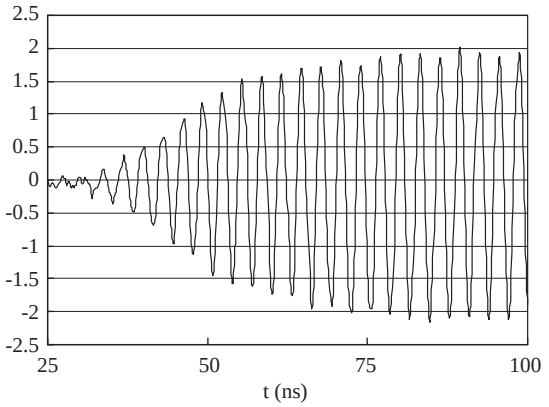

Fig. 7. Measured RF signals from the RFD cavity during the rise time. A driving power of 36 kW was used.

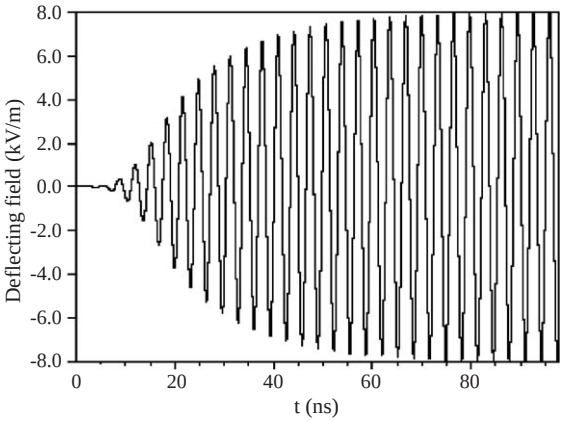

Fig. 8. Calculated RF-signal at the deflecting gap of the RFD cavity during the rise time by using the T3 module of MAFIA.

rise time of the whole RFD system was reduced to 6 periods.

To further investigate the transient behavior of the RFD cavity, a simulation was made by means of the T3 Module of MAFIA. Fig. 8 shows the calculated RF signal at the deflecting gap during the rise time. The rise time of the input signal used in the simulation was 5 RF periods, the same as that of the output signal of amplifier in the experiments. In this case, the simulated rise time is about 10 RF periods, similar as the measured result.

4. Test of the coupled RFD system

4.1. Setup of a coupled RFD system

Since the loaded Q of the RFD is very low, almost all of the driving power (~99.7%) is coupled out of an RFD cavity to a matched load. If two RFD cavities are connected so that the output power from the first RFD is utilized for the second one, the total RF power demanded for the two cavities may be halved. A coupled RFD system was proposed in the design of a chopper system for saving the cost of the RF power source [3].

Two RFDs (RFD-A and RFD-B) are connected with a coaxial cable. The coupled RFD system can be regarded as a three-cavity system: two RFD

cavities and a coaxial cavity. Because the distance between two gaps of the RFD cavities along the beam line is $3\beta\lambda$ (221.38 mm), the electric length between two cavities should be $n\lambda$ in order to keep the beam bunches synchronized with the RF field in the two RFD cavities. Here β is the relative velocity of a 3-MeV H^- ion, λ the free-space wavelength of RF, and n is an integer. The cable length was determined according to the results of a HFSS simulation. Taking the mechanical limitation in installation into account, the total cable length between two cavities is 942 mm. With this cable length, the simulated spectrum of S_{21} in Fig. 9 shows that there are three modes, in which the second mode (324 MHz) is the operating one. The phase relation between two RFD cavities can be obtained by observing the oscillation of the electric field in the two deflecting gaps by using the post processor of the HFSS. The electric field in two deflecting gaps plotted in Fig. 10 shows that the 324 MHz mode has a phase shift of $2n\pi$ between two cavities. The measured spectrum of S_{21}, depicted in Fig. 11, gives the same feature as the simulation in Fig. 9. The resonant frequency of the second mode is 323.75 MHz, with a bandwidth of 31.4 MHz and the loaded Q value of 10.4.

Because the phase relations between two cavities cannot be accurately checked by direct measurement, it is important to investigate the sensitivity of the deflecting effect with the phase error induced by the error of the connecting cable length. Table 3 gives the dependence of the displacement of a chopped beam at the position of downstream scraper of MEBT on the driving

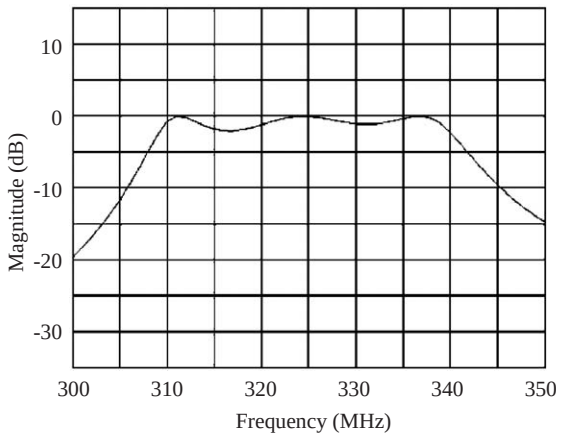

Fig. 9. Simulated S_{21} spectrum of the coupled RFD system with a connecting cable length of 942 mm.

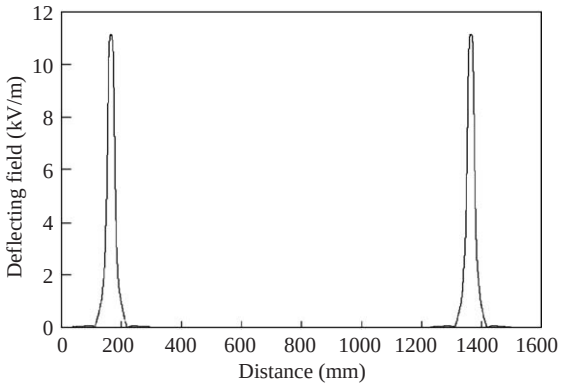

Fig. 10. Field distribution at two deflecting gaps in the coupled RFD.

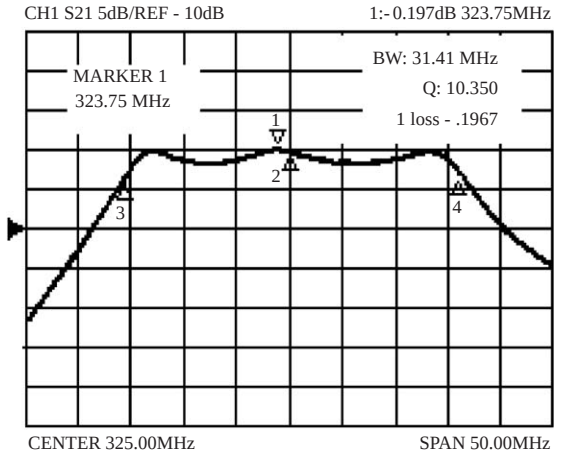

Fig. 11. Measured S_{21} spectrum of the coupled RFD system.

Table 3
Dependence of the displacement (mm) on the power and $\Delta\phi$

Driving power (kW)	$\Delta\phi$				
	0°	5.8°	10°	20°	30°
22	18.38	18.35	18.28	17.96	17.41
36	24.63	24.59	24.49	24.06	23.33

power and phase deviation ($\Delta\phi$). The results were obtained from a TRACE3D simulation of MEBT. In this simulation, an assumption was made that the reference particles always meet the peak field at RFD-A, and that the phase deviation is the phase shift from the peak field of RFD-B. This shows that, within a 10° phase deviation, the influence to the deflection effect is very small.

4.2. Study on the RF transient behavior

The rise time of the coupled RFD system is also measured by directly observing the RF response of the coupled RFD, as shown in Fig. 12, in which the dashed curve depicts the RF response from RFD-A and the solid curve the RF response from RFD-B. Similar to the case of a single RFD cavity, this measured rise time includes the contribution from the amplifier. The rise time of the first cavity (RFD-A) is about 8 RF periods, almost the same as that of a single cavity, but it becomes 11 RF periods for the second cavity (RFD-B).

In the measurement of Fig. 12, the length of the connected coaxial cable between the monitor of RFD-A and a digitizing oscilloscope was almost the same as that for RFD-B within an error of several degrees. From Fig. 12, one can find that the delay time of the second RFD excitation was about 6 RF periods. For the $3\beta\lambda$ distance between two RFD cavities along the beam line, the 6 RF periods delay means that there are three micro-bunches deflected by the first RFD only during the rise time; a similar case exists during the fall time.

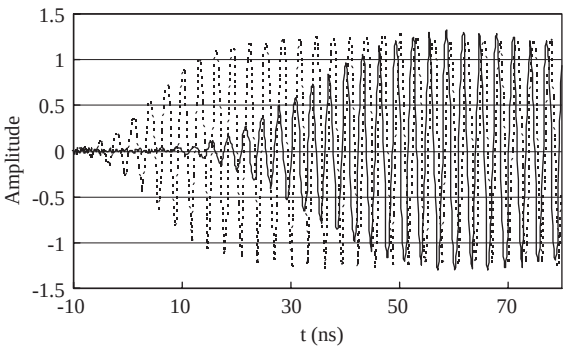

Fig. 12. Measured response of the RF pulse of a coupled RFD system. The dashed line is from the RF monitor of RFD-A, while the solid curve is from the RF monitor of RFD-B. Some delay time during transient rise time can be seen between two signals from A and B.

Detailed analyses were made on the micro-bunches deflected by the second RFD only during the transient time in the coupled RFD system [6]. The results show that the influence on the total deflecting efficiency due to the unsynchronizing excitation of two RFDs was not very large.

A similar transient behavior as that in the case of the measurement was observed in the simulation with T3 module of MAFIA, as shown in Fig. 13, in which the thin line indicates the RF signal in the gap of the RFD-A, and the dark line traces the RF signal in the gap of the RFD-B. Similar to the measurement results, the rise time of the second RFD is longer than that of the first one, and the delay time in the second RFD excitation is about 5 RF periods. The delay time obtained in the simulation is less than that in the measurement. The reason for the difference in the delay times comes from the different setups between the measurement and the simulation: in the simulation, two RFDs were connected by 50 mm coaxial cable for decreasing the required computing time, while it was connected by a 942 mm cable in the measurement.

It can be predicted that the two demerits, the longer rise time and the longer delay time in the second RFD will decrease the total deflection efficiency of the two RFD cavities. However, considering that the capability of the power amplifier is up to 36 kW, which is much larger than the demanded power of 22 kW in the design, these two demerits are not a problem, as shown in the following section on a beam test of the chopper system.

5. Beam test of the RF chopper system

An extensive beam test was performed in order to study the fundamental properties of the low-energy part of the J-PARC proton linac (a negative hydrogen ion source, a 3-MeV RFQ and the MEBT) at the beam-test stand at KEK [7]. A study of the RF chopper system is one of the important purposes of the beam test [8]. For

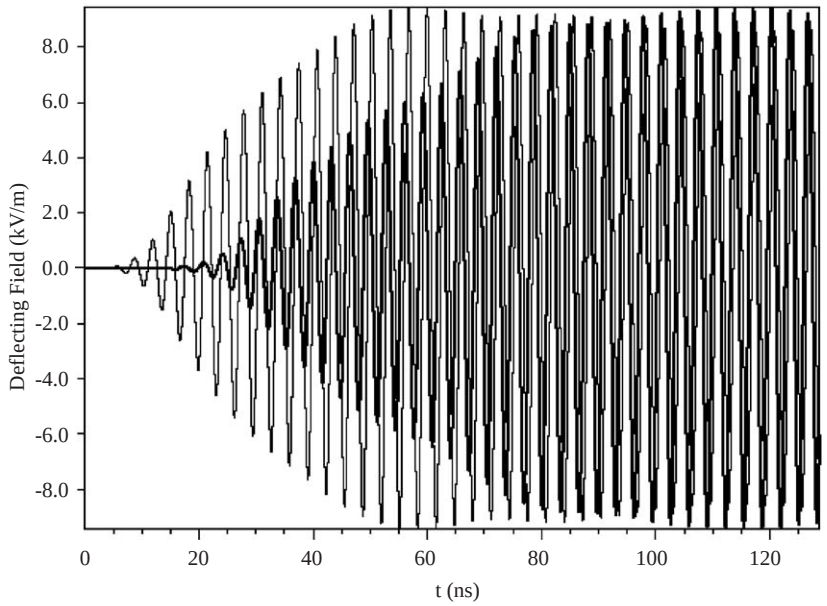

Fig. 13. Simulated response of the RF pulse of the coupled RFD system made by using the T3 module of MAFIA. The thin line indicates the RF signal in the deflecting gap of the RFD-A, and the dark line traces the RF signal in the deflecting gap of the RFD-B.

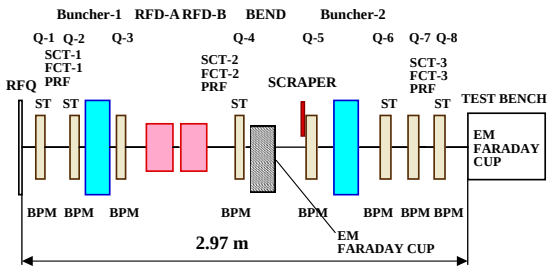

Fig. 14. Layout of the MEBT.

accomplishing beam matching and chopping, the MEBT of J-PARC includes two RFDs, two RF bunchers, eight focusing magnets, a beam scraper and several kinds of beam diagnostics (Fig. 14).

The deflecting angle depends not only on the two RFDs, but also on the fourth quadrupole of the beam line in Fig. 14, just downstream of RFD [6]. The deflection angle is initiated by the two RFDs, and then amplified more than twice by the fourth quadrupole. A long drift space, downstream of the fourth quadrupole, provides a space to generate separation between the deflected and normal beams. However, the final purpose is a large separation between the deflected beam and normal one at the beam scraper, which is located at the end of the long drift space, rather than just a large deflection. The separation also depends on the beam size at the position of the scraper, or say, depends on the setting of the beam line, especially the upstream part of the scraper. The MEBT was designed carefully to keep the small beam profile at the fourth quadrupole as well as at the position of the scraper. Based on the designed beam line, an RF power of 22 kW can produce a separation of 4.4 mm between the deflected beam and the normal one. In the beam test and operation of the MEBT, an RF driving power up to 36 kW was used for both obtaining a larger beam separation and decreasing the effective rise time during which the deflecting field reaches the required level.

5.1. Setup of the beam test

Several kinds of beam diagnostics were used in the chopped beam measurement: four slow current transformers (SCT), three fast current

transformers (FCT), eight beam position monitors (BPM), a beam scraper and a Faraday cup.

A beam scraper of tungsten was located 70 cm downstream from the second RFD. The transverse position of the scraper could be set with an accuracy of ± 0.1 mm over a range of 50 mm, and the beam current on the scraper could be measured. Taking these advantages of scraper, it was used not only as a beam stopper, but also as a monitor. The displacement of the chopped beam could be measured by using the scraper and the third SCT. Moving the scraper, when the signal of chopped part was decreased to half, the position of the scraper was regarded as the center of the chopped beam. Similarly, for the normal beam, moving the scraper to the position where just no beam was lost on the scraper, the position of the scraper was regarded as the beam size. The measured beam size on the position of the scraper was 8.8 mm, which roughly agrees with the TRACE-3D results, assuming an rms transverse emittance of 0.2π mm mrad. A scraper position of 10 mm away from the beam axis was selected for distinguishing the chopped beam from the normal one up to a beam current of 25 mA during the beam test.

The measurement of the chopped beam was made under different conditions: a low-intensity beam and a single RFD for studying the fundamental characteristics of the RF chopper system, a low-intensity beam and a coupled RFD for studying the operation of the coupled RFD system, and a high-intensity beam and a coupled RFD for studying the characteristics of the total system on realistic operation.

5.2. Measurement of the chopped beam

Fig. 15 shows the measured deflecting beam position at the position of the scraper as a function of the driving power for a single RFD-A and a coupled RFD, respectively. The measured results agree with the TRACE3D design value very well. Fig. 16 depicts a typical chopped pulse structure. One can see that the signal arising from the deflected beam, most of which was scraped by the scraper, was less than the noise level at the eighth BPM, located at the exit of the MEBT. This means

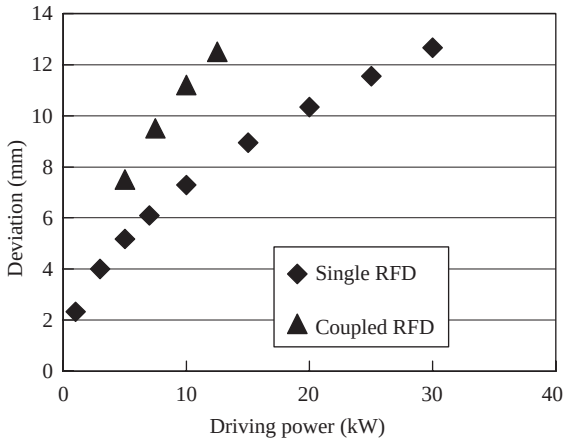

Fig. 15. Measured deflecting beam position at the scraper vs. driving RF power for both the single RFD and the coupled RFD systems.

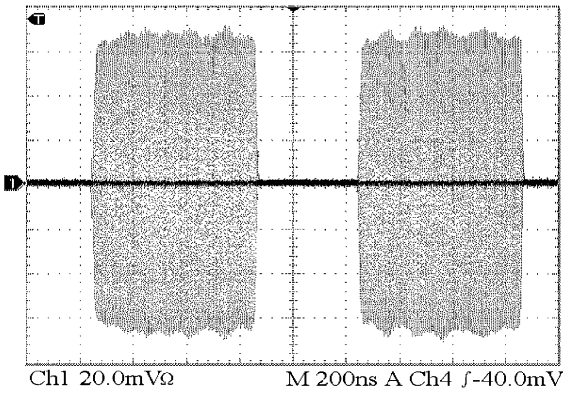

Fig. 16. Structure of a chopped beam measured by the eighth BPM. The beam current is 20 mA and $P_{in} = 36$ kW. 200 ns/div.

that the fraction of the beam at the exit of the MEBT during the chopper-on time was negligibly small.

The signal of a short chopped beam measured by the eighth BPM, during the rise time of the chopper, is shown in Fig. 17. The beam current is 24 mA and the driving power to coupled RFD system is 36 kW. The BPM detects an alternate component of the induced electromagnetic field by a microbunch. Thus, one period of a sine-like wave corresponds to a microbunch in Fig. 17. This shows that about three bunches were partly deflected during the rise time of the chopper and

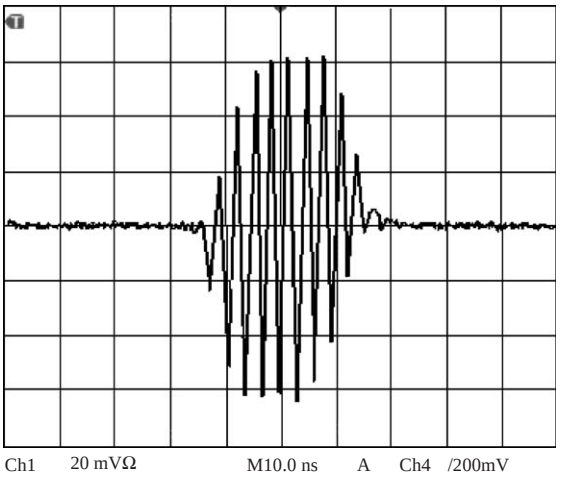

Fig. 17. Signal of a chopped beam measured by the eighth BPM The beam current is 24 mA and $P_{in} = 36$ kW. 10 ns/div. This is an example of a very short pulse with a fast rise/fall time after careful tuning of accelerating parameters.

that a part of the beam was not scraped. Benefiting from the high driving power, the rise time of the beam was about 10 ns, which is much shorter than the rise time of the coupled RFD system. In fact, in the case of 20 mA, the driving power of 22 kW was enough to produce a sufficient separation between the deflected and normal beams, but the rise time of the beam was increased to about 15 ns. The high driving power mainly contributed to shorten the rise/fall time at the head and tail of the beam pulse by enlarging the separation between the deflected beam and the normal beam.

A method for making any combination of the chopped beam of varied pulse duration or varied repetition rate was established, and very short beam pulse generated by the RF chopper system. During a beam study period of over 1 month, the RFD system is very stable and reliable in the high-power operation.

6. Discussion and conclusion

An RF chopper system consisting of two RFDs, has been successfully developed. A modification in the coupling loop of the chopper cavities was made for tuning the resonant frequency while keeping the bandwidth unchanged. In a low-level RF test, the fundamental RF properties showed good agreement with those of the design simulations. In a high-power test, the chopper worked well without any discharge under 36 kW peak driving power. The experimental and simulated results of both the rise time of the RF chopper system and the delay of the excitation of the second RFD in the coupled RFD system were compared.

The beam study of the RF chopper system shows that the RFD chopper system operates very well up to a beam current of 25 mA, satisfying the fundamental requirements for a chopped beam. The achieved rise/fall time (10 ns) of the chopped beam is close to the limit of the RF chopper system. The beam signal during chopper-on period measured at the exit of the MEBT is less than the noise level of the monitor systems. In the case of any further requirement for a faster rise/fall time of the chopped beam, we propose the following two methods: firstly, the anti-chopper system can eliminate all of the transient part of the chopped beam theoretically [9], and secondly, each RFD cavity can be independently powered with an RF source of 36 kW, so that the two demerits of the coupled RFD system, the longer rise time and the longer delay time in the second RFD, can be eliminated, and the much shorter rise time can be achieved.

Acknowledgments

The authors wish to thank Y. Yamazaki, F. Naito, S. Yamaguchi, M. Ikegami, T. Kobayashi and the linac group of J-PARC for their great support and helps. They wish to thank T. Sugano of Mitsubishi Heavy Industry for elaborate work in constructing the RFD cavities and the MEBT.

References

[1] Accelerator Technical Design Report for J-PARC, KEK Report 2002-13; JAERI-Tech 2003-044.
[2] T. Kato, New design of an RF beam chopper, Proceedings of Seventh Symposium on Accelerator Science and Technology, 1989, p. 228.
[3] S. Fu, T. Kato, Nucl. Instr. and Meth. A 440 (2000) 296.

[4] S. Wang, et al., Beam commissioning of the J-PARC Linac Medium Energy Beam Transport at KEK–II, Proceeding of the 28th Japan Linac Meeting, WP-53, Tokai, Japan, July 2003.
[5] Y. Yamaguchi, et al., Overview of the RF System for the JAERI/KEK high-intensity Proton Linac, Proceedings of 2002 International Linac Conference, Pohang, Korea, August 2002, p. 452.
[6] S. Fu, T. Kato, Nucl. Instr. and Meth. A 457 (2001) 423.
[7] M. Ikegami, et al., Beam commissioning of the J-PARC Linac medium energy beam transport at KEK, Proceedings of PAC2003, Portland, USA, May 2003, p. 1509.
[8] T. Kato, et al., Beam study with RF choppers in the MEBT of the J-PARC Proton Linac, Proceedings of PAC2003, Portland, USA, May 2003, p. 1455.
[9] S. Wang, S. Fu, T. Kato, Design study of A MEBT with an anti-chopper for the JKJ, Proceedings of 2002 International Linac Conference, Pohang, Korea, August 2002, p. 79.